frontiers in
MICROBIOLOGY

ORIGINAL RESEARCH ARTICLE
published: 13 April 2011
doi: 10.3389/fmicb.2011.00071

Structural insights into dissimilatory sulfite reductases: structure of desulforubidin from *Desulfomicrobium norvegicum*

Tânia F. Oliveira[1,2], Edward Franklin[2], José P. Afonso[3], Amir R. Khan[2], Neil J. Oldham[3], Inês A. C. Pereira[1]* and Margarida Archer[1]*

[1] *Instituto de Tecnologia Química e Biológica, Universidade Nova de Lisboa, Oeiras, Portugal*
[2] *School of Biochemistry and Immunology, Trinity College, Dublin, Ireland*
[3] *School of Chemistry, University of Nottingham, Nottingham, UK*

Edited by:
Martin G. Klotz, University of Louisville, USA

Reviewed by:
John Robert Cort, Pacific Northwest National Laboratory, USA
Vilmos Fulop, University of Warwick, UK

****Correspondence:***
Margarida Archer, Membrane Protein Crystallography Laboratory, Instituto de Tecnologia Química e Biológica, Universidade Nova de Lisboa, Avenida da República EAN, 2780-157 Oeiras, Portugal.
e-mail: archer@itqb.unl.pt;
Inês A. C. Pereira, Bacterial Energy Metabolism Laboratory, Instituto de Tecnologia Química e Biológica, Universidade Nova de Lisboa, Avenida da República EAN, 2780-157 Oeiras, Portugal.
e-mail: ipereira@itqb.unl.pt

Dissimilatory sulfite reductases (dSiRs) are crucial enzymes in bacterial sulfur-based energy metabolism, which are likely to have been present in some of the earliest life forms on Earth. Several classes of dSiRs have been proposed on the basis of different biochemical and spectroscopic properties, but it is not clear whether this corresponds to actual physiological or structural differences. Here, we describe the first structure of a dSiR from the desulforubidin class isolated from *Desulfomicrobium norvegicum*. The desulforubidin (Drub) structure is assembled as $\alpha_2\beta_2\gamma_2$, in which two DsrC proteins are bound to the core $[DsrA]_2[DsrB]_2$ unit, as reported for the desulfoviridin (Dvir) structure from *Desulfovibrio vulgaris*. Unlike Dvir, four sirohemes and eight [4Fe–4S] clusters are present in Drub. However, the structure indicates that only two of the Drub coupled siroheme-[4Fe–4S] cofactors are catalytically active. Mass spectrometry studies of purified Drub and Dvir show that both proteins present different oligomeric complex forms that bind two, one, or no DsrC proteins, providing an explanation for conflicting spectroscopic and biochemical results in the literature, and further indicating that DsrC is not a subunit of dSiR, but rather a protein with which it interacts.

Keywords: sulfite reductases, sulfur metabolism, sulfate reducing bacteria, siroheme, iron–sulfur clusters, X-ray structure

INTRODUCTION

Microorganisms play an important role in sulfur transformations and are a critical component of sulfur cycling on our planet. Many Bacteria and Archaea have the ability to use sulfur compounds in a series of oxidation or reduction reactions, thereby generating metabolic energy in the process of dissimilatory metabolism. Data from isotopic analysis suggests that dissimilatory reduction of sulfur compounds is an extremely ancient process which began 3.5 billion years ago (Canfield and Raiswell, 1999; Canfield et al., 2006). After sulfate concentrations increased significantly in the Precambrian oceans approximately 2.5 billion years ago, reduction of sulfate also became of global significance (Canfield et al., 2006). A key enzyme in the reduction of sulfate/sulfite is the dissimilatory sulfite reductase (dSiR), which is responsible for the six electron reduction of sulfite to sulfide. dSiRs belong to a redox enzyme super family, characterized by the presence of a coupled siroheme-[4Fe–4S] cluster cofactor, which include assimilatory sulfite (aSiRs) and nitrite reductases, and other types of sulfite reductases (Crane and Getzoff, 1996; Dhillon et al., 2005; Loy et al., 2007). The dSiR is composed of two subunits, DsrA and DsrB, in a ~200 kDa $\alpha_2\beta_2$ arrangement. The *dsrA* and *dsrB* genes are paralogous and probably originated from duplication of an early *dsr* gene before the separation of the Archaea and Bacteria domains (Dahl et al., 1993; Molitor et al., 1998; Wagner et al., 1998). aSiRs, which generate sulfide for incorporation into amino-acids and cofactors, are monomeric enzymes with an internal two-fold symmetry of a unit related to DsrA/DsrB, which suggests gene duplication, followed by gene fusion of an ancestral sulfite reductase gene present in a very early life form (Crane et al., 1995, 1996; Dhillon et al., 2005). After the early divergence of the aSiR and dSiR genes there was incorporation of a ferredoxin domain in the *dsr* gene before separation into the *dsrA* and *dsrB* genes (Dahl et al., 1993). Evolutionary analysis of the *dsrAB* genes indicates they were mainly inherited via vertical transmission, except for a few events of lateral gene transfer, namely in the archaeal genus *Archaeoglobus*, which has *dsrAB* genes of bacterial origin, in the thermophilic genus *Thermodesulfobacterium*, and Gram-positive bacteria of the *Firmicutes* phylum like *Desulfotomaculum* species (Wagner et al., 1998; Klein et al., 2001; Zverlov et al., 2005; Loy et al., 2007). In contrast to aSiRs, which reduce sulfite directly to sulfide, the *in vitro* product of dSiRs is not only sulfide, but a mixture of products including also trithionate and thiosulfate (Peck and LeGall 1982), suggesting other proteins may be required for the complete reduction to sulfide. Thus, the mechanism and physiological products of dissimilatory reduction by dSiRs is still a matter of debate.

Biochemical studies of dSiRs led to their categorization into four different classes based on UV/visible absorption and other molecular characteristics (Rabus et al., 2007): Desulfoviridin (Dvir), a green protein (characteristic absorption peak at 628 nm) present in *Desulfovibrio* spp. (Lee and Peck, 1971; Moura et al., 1988; Pierik and Hagen, 1991; Steuber et al., 1994; Wolfe et al., 1994); Desulforubidin (Drub), a reddish-brown protein (characteristic absorption peak at 545 nm) present in *Desulfomicrobium* and *Desulfosarcina* spp. (Lee et al., 1973; Moura et al., 1988; Arendsen et al., 1993; DerVartanian, 1994); Desulfofuscidin (characteristic absorption peak at 576 nm) present in *Thermodesulfobacterium* spp. (Hatchikian and Zeikus, 1983; Hatchikian, 1994); and the brown colored P-582 protein (characteristic absorption peak at 582 nm) present in *Desulfotomaculum* spp. (Akagi et al., 1974). All these dSiRs are proposed to assemble as $\alpha_2\beta_2$, but the type and content of the cofactors has been the subject of some controversy (Rabus et al., 2007).

After many years of failed attempts, the first X-ray structures of dSiRs were determined, including the Dvir from *Desulfovibrio vulgaris* Hildenborough at 2.10 Å (Oliveira et al., 2008a), and dSiR from *Archaeoglobus fulgidus* at 2.04 Å resolution (Schiffer et al., 2008), showing an $\alpha_2\beta_2$ arrangement with similar overall folds, and finally shedding light on the cofactor composition of these proteins. Four sirohemes and eight [4Fe–4S] clusters are present in *A. fulgidus* dSiR, whereas two sirohemes, two sirohydrochlorins (the metal-free form of siroheme), and eight [4Fe–4S] clusters are present in *D. vulgaris* Dvir. Nevertheless, only two sirohemes per $\alpha_2\beta_2$ unit are proposed to be catalytically active in both proteins. The sequence-based predictions of a similar fold to aSiRs, and of a separate ferredoxin domain containing a [4Fe–4S] cluster that transfers electrons to the active site, were confirmed by these structures. In addition, the crystal structure of *D. vulgaris* Dvir provided important functional information, because it comprised the DsrAB subunits complexed with the DsrC protein in a $\alpha_2\beta_2\gamma_2$ arrangement. DsrC was originally thought to constitute a third subunit of dSiR (Pierik et al., 1992), but has subsequently been recognized as an independent protein that interacts with DsrAB (Steuber et al., 1995; Cort et al., 2001, 2008; Dahl et al., 2005; Mander et al., 2005; Pires et al., 2006), and is homologous to the TusE protein involved in biosynthetic sulfur-relay reactions (Ikeuchi et al., 2006; Numata et al., 2006). In the structure of the *D. vulgaris* DsrAB–DsrC complex, the strictly conserved Cys at the C-terminus of DsrC is positioned right next to the substrate-binding site pointing to the involvement of DsrC in the reduction of sulfite (Oliveira et al., 2008a).

More recently, the crystal structure of the Dvir from *Desulfovibrio gigas* has been reported in two active forms (Dvir-I and Dvir-II; Hsieh et al., 2010), also including the DsrAB and DsrC proteins. The overall structure of the two *D. gigas* Dvir forms are very similar to *D. vulgaris* Dvir, and the C-terminal tail of DrsC from both forms is either inserted into the channel formed between DsrA and DsrB or swung away from the catalytic siroheme (Hsieh et al., 2010). *D. gigas* Dvir belongs to the Dvir class, and comprises eight iron–sulfur clusters, two sirohemes, and two sirohydrochlorins, as reported for Dvir. However, Dsr-II contains a [3Fe–4S] cluster associated with the siroheme instead of the usual [4Fe–4S] center, observed in all the other structures analyzed so far. Additionally, the *A. fulgidus* DsrAB structure has been characterized in complex with several ligands (Parey et al., 2010).

In this work we report the 3D structure of a dSir from a different class, the Drub isolated from *Desulfomicrobium norvegicum*, at 2.5 Å resolution. Moreover, we report mass spectrometry studies of both Drub and Dvir that provide important insights into the quaternary structures of these proteins in solution.

MATERIALS AND METHODS

PROTEIN PURIFICATION

Desulfomicrobium norvegicum (formerly known as *Desulfovibrio desulfuricans* strain Norway 4 and *Desulfovibrio baculatus* strain Norway 4) was grown in lactate/sulfate medium and cell extracts prepared as previously described (Pereira et al., 2006). The purification protocol was performed aerobically at 6°C. The soluble fraction was loaded on a DEAE-Sepharose fast flow XK50/30 column (GE Healthcare) equilibrated with 20 mM Tris–HCl pH 7.6 buffer. A stepwise gradient of increasing NaCl concentration (0 to 1 M, incremental steps of 0.05 M) was performed. The fraction eluted with 300 mM NaCl was dialyzed against 20 mM Tris–HCl pH 7.6. The protein was then concentrated and loaded onto a Q-Sepharose 26/10 ion-exchange column (GE Healthcare), and a similar procedure was performed. The protein sample was then subjected to size exclusion chromatography on a Sephacryl S-200 HR (GE Healthcare). Finally, the protein was dialyzed in 20 mM Tris–HCl pH 7.6 and loaded onto a Mono Q 5/50 GL column (GE Healthcare) and eluted using the same NaCl step gradient as outlined above. All purification steps were monitored by Sodium Dodecyl Sulfate Polyacrylamide Gel Electrophoresis (SDS-PAGE) and UV–visible spectroscopy analysis.

CRYSTALLIZATION

The protein was concentrated with Amicon (100 kDa cutoff) to 8 mg ml^{-1} in 20 mM Tris–HCl pH 7.6 and was further used for crystallization trials with a TTP LabTech's mosquito nanoliter pipetting crystallization robot. Many screens were tested (PEG I and II from Qiagen; Structure Screen, Pact Premier I and II, and JSCG from Molecular Dimensions; Wizard I and II and JBS screen HTS L I and II from Jena Biosciences) with some initial crystals being obtained. Crystal optimization was complicated due to poor crystal reproducibility between different batches of purified protein, and protein degradation over time. Thin needle crystals were obtained using the hanging drop vapor diffusion method at 291 K with a reservoir volume of 500 µl of 20% PEG 3350 (w/v), 0.1 M BisTris Propane pH 7.5, and 0.2 M K/Na Tartrate. Crystals grew using a protein: precipitant ratio of 2:1 (total volume of 3 µl) over 2 months with dimensions of 0.15 mm × 0.03 mm × 0.03 mm. Prior to X-ray data collection, crystals were cryo-protected by being briefly dipped into a reservoir solution supplemented with 25% glycerol, and immediately flash-cooled in liquid nitrogen.

DATA COLLECTION AND STRUCTURE DETERMINATION

X-ray diffraction data were collected at 0.933 Å at ID14-2 beamline, ESRF – Grenoble, France, to 2.5 Å resolution. A total of 340 images were measured with an oscillation range of 0.6° and exposure time

of 10 s per image. Data were processed with *MOSFLM* (Leslie, 1992); and scaled with *SCALA* from the *CCP4* program suite (Collaborative Computational project, Number 4, 1994). The sequence information for *D. norvegicum dsrAB* genes is incomplete at their termini. They do however share 99% sequence identity with the corresponding genes of *Desulfomicrobium baculatum* (strain DSM 4028). This high identity allowed completion of the Drub *dsrAB* sequences based on those from *D. baculatum*: 62 amino-acid residues were added at the N-terminus of DsrA and 115 residues at the C-terminus of DsrB.

Molecular Replacement was done with *PHASER* (McCoy et al., 2007) using the *D. vulgaris* Dvir (PDB code: 2V4J; Oliveira et al., 2008a) as a search model. One *PHASER* run was performed searching independently for two molecules of each Dsr-A, B, and C subunits. A solution was obtained with rotation (RFZ) and translation functions (TFZ) of 22.9 and 23.1, respectively, and a refinement log-likelihood gain LLG of 662.90.

A first model building cycle was performed with *BUCANEER* (Cowtan, 2006). Electron-density map inspection and manual model building were carried out using *COOT* (Emsley and Cowtan, 2004). Further refinement was done with *REFMAC5* (Murshudov et al., 1997) within the *CCP4* program suite. For the refinement a subset (5%) of the reflections were randomly excluded for cross validation (R_{free} calculation). All structural figures were drawn with *PyMOL* (DeLano, 2002).

The atomic coordinates and structure factors of Drub isolated from *D. norvegicum* were deposited in the RCSB Protein Data Bank with accession number 2XSJ.

MASS SPECTROMETRY STUDIES

Purified *D. norvegicum* Drub and *D. vulgaris* Dvir were subjected to preparative 9% native gel electrophoresis. Each band was excised from the gel and the protein extracted by electro-elution as described in (Oliveira et al., 2008b). Nanoflow electrospray ionization-mass spectrometry was performed on the proteins thus obtained. Experiments were conducted on a Waters Synapt High Definition Mass Spectrometer (Manchester, UK) – a hybrid quadrupole/ion mobility/orthogonal acceleration time of flight (oa–TOF) instrument – equipped with a nanospray source and operated in TOF mode. Protein samples were buffer-exchanged into 1 M ammonium acetate pH 7.5 buffer using Vivaspin 500 centrifugal filters with 10 kDa molecular weight cutoff (Sartorius, Göttingen, Germany), diluted to a final concentration of 5 μM and electrosprayed from thin wall Nanoflow Probe Tips (Waters, Manchester, UK). Experiments were conducted at a capillary voltage of 1.5 kV, nanoflow gas pressure of 0.3 Bar, source temperature of 323 K, and sample cone voltage of 30 V, with the source operating in positive ion mode. Backing pressure was maintained between 5.0 and 6.0 mBar to provide collisional cooling of ions in the intermediated vacuum region of the instrument. The collisional energies were 50–70 V in the trap and 30–50 V in the transfer, with a trap gas flow of 10 ml min^{-1} resulting in a pressure of 5.2×10^{-2} mBar. Tandem mass spectrometry experiments were performed with trap voltages between 60 and 120 V. The oa-TOF-MS was operated over the scanning range of m/z 500–15000. Spectra were acquired and processed using Masslynx 4.1 software (Waters, Manchester, UK).

ELECTRON TRANSFER ASSAYS

Desulfoviridin from *D. vulgaris* Hildenborough was used in experiments to test potential electron donors, since it can be purified with much higher yields than Drub from *D. norvegicum*. Direct protein–protein interactions were probed using the surface plasmon resonance technique (Biacore T100 GE Healthcare). Two possible electron donors were tested: ferredoxin-I (FDX; DVU3276) isolated from *D. vulgaris* Hildenborough, and pyruvate–ferredoxin oxidoreductase (PFOR) isolated from *Desulfovibrio africanus* (as the *D. vulgaris* one is very unstable and shows 69/82% sequence identity/homology with *D. vulgaris* protein). A CM5 (carboxymethylated dextran) chip from GE Healthcare was used for the immobilization of dSiR *D. vulgaris*, and FDX and PFOR were tested as analytes. In one of the cases, the reverse experiment was performed, with FDX being coupled to the CM5 chip and *D. vulgaris* dSiR used as analyte.

Reduction of sulfite by Dvir with pyruvate/PFOR as electron donors was followed by spectroscopic measurement of hydrogen sulfide, using an adaptation of the methylene blue (MB) method (Fogo and Milton, 1949). MB is produced when sulfide reacts with *N*,*N*′-dimethyl-*p*-phenylenediamine (DPD) and ferric chloride under acidic conditions. For the assay, the reaction mixture contained 10 mM sodium pyruvate, 100 μM coenzyme A, 22.5 nM PFOR, 625 nM Dvir, and 200 μM sodium sulfite in a total volume of 200 μl and was started with the addition of sulfite and stopped at various time points (30min, 1 h, 2 h, 3 h, 4 h, and 12 h) on addition of 50 μl of the DPD/$FeCl_3$ mixture (prepared in 50% HCl). The color was allowed to develop by incubating at room temperature for 10 min before the absorbance was measured at 670 nm in a 96 well plate on a SpectraMax Plus384 spectrophotometer.

RESULTS AND DISCUSSION

DRUB CRYSTAL STRUCTURE

The purified sample of *D. norvegicum* Drub showed three bands in SDS-PAGE analysis corresponding to DsrA, DsrB, and DsrC protein, as also reported for other dSiRs (Pierik et al., 1992; Steuber et al., 1995). Crystals of Drub were obtained using PEG3350 as precipitant (pH ~7.5) and diffracted to ~2.5 Å at a synchrotron source. Drub crystals belonged to the orthorhombic space group ($P2_12_12_1$) with unit cell dimensions $a = 99.3$, $b = 135.1$, and $c = 178.0$ Å. The Matthews coefficient (Matthews, 1968) was 2.7 $Å^3$ Da^{-1}, consistent with the presence of one molecule ($\alpha_2\beta_2\gamma_2$) in the asymmetric unit and 53.3% of solvent content. The structure of Drub was determined by molecular replacement using the coordinates of *D. vulgaris* Dvir as search model.

The final crystallographic model of Drub comprised 1850 amino-acid residues out of 1856, 4 sirohemes and 8 [4Fe–4S] clusters, 2 sulfite ions, 1 glycerol, and 1051 water molecules (**Figure 1**). Final refinement values for R and R_{free} are 15.6 and 20.8%, respectively, with the entire model fitting the generally well defined electron-density map.

The deposited sequences for *D. norvegicum dsrA* and *dsrB* genes are incomplete at the N-terminal of *dsrA* and C-terminal of *dsrB*. However, due to the very high sequence identity (~99%) with *D. baculatum dsrAB* genes, the sequences of *D. norvegicum dsrA* and *dsrB* were completed. On inspection of the inserted residues extrapolated from the sequence of *D. baculatum*, six residues were observed which did not fit the electron-density and thus were not

conserved in the *D. norvegicum* sequences. Amino-acid residues at positions 33A, 57A, and 59A were refined manually with serine providing the best fit, residue 35A was refined as Gln, 323B as Ser and 364B as Ile, taking also into account their chemical environments. These predictions are expected to be robust, but nevertheless potential mis-assignments will not have major implications for the structural model due to the nature and position of these residues. Structure analysis and validation of the model was achieved using *PROCHECK* (Laskowski et al., 1993) from CCP4 indicating good stereochemistry. The relevant statistics for data processing and structure refinement are displayed in **Table 1**.

OVERALL DRUB ARCHITECTURE AND COFACTORS

The overall structure of *D. norvegicum* Drub (**Figure 1**) forms a dimer of αβγ units with a MW of 200 kDa. The $\alpha_2\beta_2\gamma_2$ unit corresponding to $[DsrA]_2[DsrB]_2[DsrC]_2$ is composed of the α subunit comprising residues 2–437 of chains A and D, the β subunit consisting of residues 2–386 from chains B and E, and the γ subunit containing residues 2–105 of chains C and F. In some dSiRs, namely Dvirs, the small DsrC protein copurifies with DsrAB (Pierik et al., 1992; Steuber et al., 1995), whereas in other dSiRs it does not (Dahl et al., 1993; Molitor et al., 1998).

The C-terminal arm of DsrA (405–437 of chains A/D) extends toward DsrB from the other monomer (DsrB*, chains E/B), and establishes several hydrogen-bonds with amino-acid residues from this subunit, important for dimer stabilization. Both DsrA and DsrB proteins are formed by three domains ($A_1A_2A_3/B_1B_2B_3$) as observed in *D. vulgaris* (Oliveira et al., 2008a), *A. fulgidus* (Schiffer et al., 2008), and *D. gigas* (Hsieh et al., 2010) dSiRs. The Drub structure comprises a conserved four domain core ($A_1A_2B_1B_2$, where A_1 corresponds to residues 19A–168A, A_2 to 169A–241A and 135B–207B, B_1 to residues 24B–134B, and B_2 to residues 323A–402A and 283B–370B) that is homologous to the structures of aSiRs and aNiR (Crane et al., 1995; Schnell et al., 2005; Swamy et al., 2005).

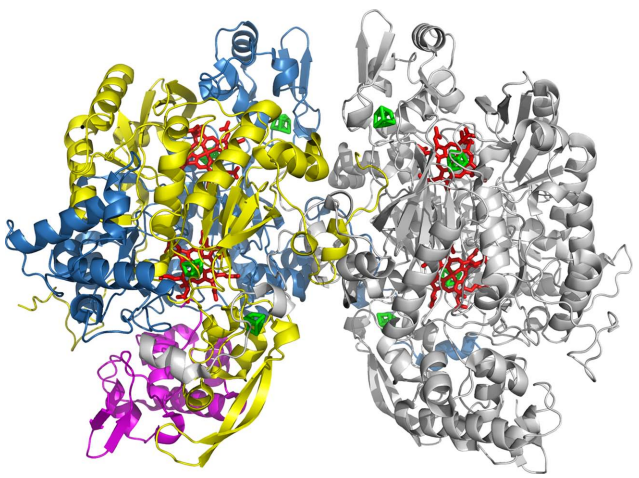

FIGURE 1 | Cartoon representation of the overall $\alpha_2\beta_2\gamma_2$ structure of Drub from *D. norvegicum*. α (DsrA) is colored in blue, β (DsrB) in yellow, and γ (DsrC) in magenta for one αβγ unit (chains D, E, and F), whereas the other is displayed in gray (chains A, B, and C). Sirohemes and [4Fe–4S] clusters and are represented in sticks and colored respectively red and green.

A third ferredoxin domain A_3/B_3 is present in both DsrA and DsrB, where A_3 consists of residues 242A–322A, and B_3 refers to residues 208B–282B.

Table 1 | Data collection and refinement statistics.

Data collection and processing	
Beamline	ID14-2 ESRF, Grenoble
Wavelength (Å)	0.933
Resolution range (Å)	45.10–2.53 (2.67–2.53)
No of images	340
Space group	$P2_12_12_1$
Unit cell parameters (Å)	a = 99.3, b = 135.1, c = 178.0
Mosaicity (°)	0.4
No. of complexes in asymmetric unit	1 ($\alpha_2\beta_2\gamma_2$)
R_{merge} (%)[a]	11.4 (28.6)
R_{pim} (%)[b]	4.2 (11.1)
$I/\sigma(I)$	12.8 (5.8)
Multiplicity	8.1 (7.4)
Completeness (%)	99.4 (96.9)
Total reflections	649457 (82716)
Unique reflections	79925 (11215)
Wilson B (Å^2)	33.5
Refinement	
No. of amino-acid residues	1850
Other molecules	
Siroheme (SRM)	4
[4Fe–4S]	8
SO_3^{2-}	2
Glycerol	1
Water molecules	1051
R (working set) (%)	15.6
R_{free} (%)	20.8
Ramachandran plot, residues in	
Most favored regions (%)	88.5
Additional allowed regions (%)	11.0
Generously allowed regions (%)	0.3
Disallowed regions (%)	0.3
Average B-factor (Å^2)	
Main chain	
DsrAB	13.6
DsrC	26.7
Side-chain	
DsrAB	14.9
DsrC	28.7
Solvent molecules	18.0
r.m.s. deviation from ideal values	
Bond length (Å)	0.015
Bond angle (°)	1.56

Values in parentheses are for the outer shell.

(a) $R_{merge} = \sum_{hkl}\sum_i \left| I_i(hkl) - \overline{I(hkl)} \right| \Big/ \sum_{hkl}\sum_i I_i(hkl)$

(b) $R_{pim} = \sum_{hkl}\left[1/(N-1) \right]^{1/2} \sum_i \left| I_i(hkl) - \overline{I(hkl)} \right| \Big/ \sum_{hkl}\sum_i I_i(hkl)$

Calculated with the program SCALA, R_{merge}, and R_{pim} are indicators of the precision of the final merged and averaged data-set, where $I_i(hkl)$ is the observed intensity of the ith measurement, $\overline{I(hkl)}$ is the average intensity of multiple observations of symmetry-related reflections and N is redundancy.

Each of the A_2/B_2 domains binds a saddle-shaped siroheme-[4Fe–4S] cofactor, giving a total of four sirohemes per $\alpha_2\beta_2$ unit as described for the dSiR of *A. fulgidus* (**Figure 2**). In contrast, dSiRs from *D. vulgaris* and *D. gigas* contain two sirohemes and two flat sirohydrochlorins per $\alpha_2\beta_2$ unit. The [4Fe–4S] cluster of the coupled siroheme cofactor in A_2 is coordinated by the strictly conserved Cys-X_5-Cys-X_n-Cys-X_3-Cys motif (Cys residues 177A, 183A, 221A, and 225A), whereas a different cysteine motif (C-X_n-C-C-X_3-C) is observed in the B_2 domain (Cys residues 151B, 188B, 189B, and 193B). In each motif two cysteine residues (225A and 193B) share the coordination of the [4Fe–4S] cluster and the siroheme. In the A_3/B_3 ferredoxin domains the [4Fe–4S] cluster is coordinated by cysteines 283A, 303A, 306A, and 309A; and 231B, 263B, 266B, and 269B, respectively. Previous cofactor quantifications of dSiRs from the Drub class indicated a content of 2.2 ± 0.3 mol of siroheme and 21 ± 2 mol of iron per mol of *D. baculatum* Drub (Moura et al., 1988), and 2 sirohemes and approximately 15 irons for *Desulfosarcina variabilis* Drub (Arendsen et al., 1993). The present structure indicates these values were underestimated with a total of 4 sirohemes, 36 irons, and 32 sulfurs present in the *D. norvegicum* Drub $\alpha_2\beta_2$ unit.

The structure of DsrC is mainly helical and comprises 104 residues out of 105. The C-terminal arm of DsrC (Leu98C–Val105C) is inserted into a cleft between DsrA and DsrB, which leads into the active site, with the conserved terminal cysteine (Sγ Cys104C/E) covalently linked to the catalytic siroheme (20′-*meso* carbon of the porphyrin ring; **Figure 2**). This covalent interaction was also observed in *D. vulgaris* (Oliveira et al., 2008a) and more recently in *D. gigas* Dvirs (Hsieh et al., 2010). We proposed that the covalent Cys104C-siroheme bond is non-physiological and forms as a result of porphyrin oxidation to give a π-cation radical that is quenched by the nearby Cys (Oliveira et al., 2008a). The presence of this bond probably stabilizes the DsrAB–DsrC complex and facilitates crystallization.

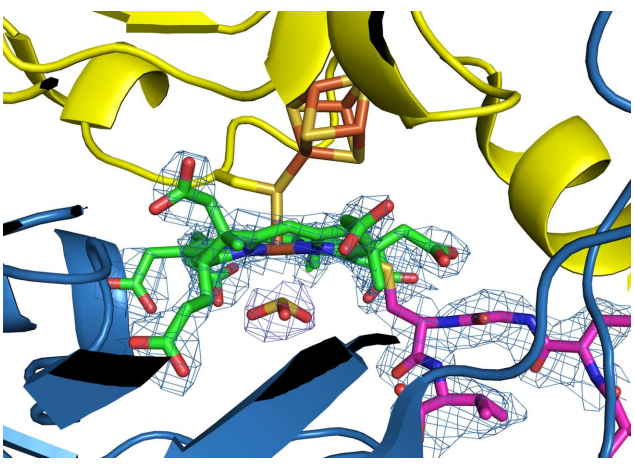

FIGURE 2 | Zoomed view of siroheme B – [4Fe–4S] cluster bridged by a cysteine residue (Cys193B). The covalent bond between Cys104C (DrsC is magenta) and siroheme B is displayed. A SO_3^{2-} is observed at the distal site of the catalytic siroheme. The 2Fo–Fc electron-density map is contoured at 1.5σ. DsrA is displayed in blue and DsrB in yellow. Atom color code: C, green; N, blue; Fe, orange; S, gold, and O, red.

Interestingly, two other DsrC conformations are observed in the recently reported *D. gigas* Dvir structure: in one there is no covalent bond between Cys104C and the siroheme and the cysteine side-chain is closer to the sulfite present in the active site; in the other one, the DsrC C-terminal arm is swung away from the siroheme in a way that brings Cys104C close to Cys93C (3.4–4.0 Å apart), but not forming a disulfide bond (Hsieh et al., 2010). In 70% of the molecules the DsrC arm is in the extended configuration, and in 30% in the retracted one, but both conformations are proposed to be in dynamic equilibrium (Hsieh et al., 2010). Previous crystal and solution structures of isolated DsrC proteins have also shown flexibility around the C-terminal tail, with either extended or retracted conformations (Cort et al., 2001, 2008; Weiss et al., 2004; Mander et al., 2005). Structural analysis of *D. gigas* Dvir reveals that Pro101C suffers significant conformational changes between these two conformations, functioning as a hinge, and being responsible for the different positions of the C-terminal arm (Pro-Thr-Gly-Cys-Val). There is enough space around the C-terminal tail in the DsrAB cleft to accommodate such structural rearrangements, while the rest of the DsrC globular domain and the DsrAB structure remain basically the same regardless of the DsrC C-terminal segment conformation. The presence of these two alternative conformations of the DsrC arm in the *D. gigas* Dvir structure provide supporting evidence for our proposal that the DsrC penultimate Cys is involved in the catalytic cycle and that a disulfide bond is ultimately formed between the two conserved DsrC cysteines (Oliveira et al., 2008a).

THE CATALYTIC SITE

The catalytic siroheme-bound by DsrB is buried in the protein interior and sits at the interface between DsrA and DsrB (**Figure 2**). DsrA provides the basic residues for substrate-binding at the distal site, whereas DrsB supplies the residues at the proximal site including Cys193B. This cysteine residue is covalently bound to the siroheme iron (~2.3 Å) and a cluster iron (~2.5 Å), where both irons are *ca.* 4.3 Å apart. The [4Fe–4S] cluster is bound exclusively by residues from DsrB subunit. A blob of electron-density with a trigonal pyramidal shape is observed at the distal site of the siroheme iron suggesting an axial ligand bound to it. A sulfite ion (SO_3^{2-}) was modeled into the blob with its sulfur pointing toward the siroheme moiety (sulfur atom is at a distance of ~2.3 Å to the siroheme iron, **Figure 2**). Arg101A, Arg172A, Lys213A, and Lys215A are strictly conserved residues that interact directly with the substrate. These residues together with other basic residues, such as arginines (83A, 231A, 376A, 378A, and 71B), lysine 217A, and histidines (150B and 152B) form a positively charged pocket with a favorable environment for binding the negatively charged sulfite and compensate the negative charges of the siroheme carboxylate groups (propionates and acetates substituents). The identification of the substrate channel leading to the catalytic siroheme is not consensual. A 15-Å long channel was identified in *A. fulgidus* dSiR (DsrAB), involving Arg80A, Arg358A, His64A, and His141B, with a size of 10 × 15 Å at its entrance and *ca* 6 × 9 Å at its substrate-binding pocket (Schiffer et al., 2008), This large cavity is however almost completely occupied by the C-terminal arm of DsrC, which is not present in *A. fulgidus* dSiR. Beside this channel, a narrower funnel is observed in Drub with a positive electrostatic potential which makes the distal side of the catalytic siroheme solvent accessible. The entrance is formed by Tyr212A, Arg376A, Glu381A

Leu226B, and is not blocked by the DsrC binding. This putative substrate funnel is also present in the other dSiR structures. In *D. gigas* Dvir, two other possible entry points are proposed: channel A, where Lys100C can bind a sulfite at the surface and transfer it to the active site through a swing of the DsrC C-terminal arm; and channel B which can connect the sirohydrochlorin and siroheme within each monomer, with Cys198B and Arg231A located in the middle of the channel (Hsieh et al., 2010). More structural and functional information is needed to clarify this issue.

Despite the presence of four siroheme-[4Fe–4S] cofactors in Drub, the sirohemes bound by DsrA should not be catalytically active, because they are not solvent accessible, and several basic residues important for substrate-binding are missing at the distal side of the heme. *D. vulgaris* and *D. gigas* Dvirs contain sirohydrochlorin at this site in DsrA, whereas *A. fulgidus* also has a siroheme. Interestingly, in aSiRs this second cofactor-binding site is empty.

STRUCTURAL COMPARISON OF DRUB WITH OTHERS dSiRs

Superposition of Drub with other dSiR structures from *D. vulgaris*, *D. gigas*, and *A. fulgidus* with PDBeFold (Krissinel and Henrick, 2004) yielded root-mean-square (r.m.s.) deviations of 0.74, 0.8, and 1.37Å for 1830, 1837, and 1500 aligned Cα atoms, respectively. Drub shares 74, 72, and 53% of amino-acid sequence identity with *D. vulgaris*, *D. gigas*, and *A. fulgidus* dSiRs, respectively.

Although the overall fold of dSiRs is quite conserved, there are some relevant localized differences (**Figure 3**). In Drub, DsrB has an inserted loop formed by residues 239B and 254B (5 residues longer than in *D. vulgaris* and *D. gigas* Dvirs, and 11 residues longer than *A. fulgidus* dSiR), which corresponds to a longer two stranded anti-parallel β-sheet followed by a three-residue-H-bonded turn. This loop extends outward in between the N-terminal of DsrA* (chain D) and DsrC. Moreover, the DsrB N-terminus of Drub is 11-residues longer than in *A. fulgidus* dSiR, but similar to *D. vulgaris* and *D. gigas* Dvir. It adopts an extended conformation toward DsrA residues: 39A–41A (located in a bending loop, e.g., the distance between the Cαs of 3B–41A is 5.9 Å), and 147A–151A (sited in a α-helix, Cα distance of 6B–151A is 5.3 Å); and DsrC (e.g., O atom of Pro10B is 5.9 Å apart from Oε1 Glu35C, Cγ of Pro13B is 4.7 Å away from Cα Gly38C). The O atom of Val4B and Asn16B are establishing hydrogen-bonds with the side-chain atoms of Arg125A and His158A, respectively. Interestingly, both of these inserted segments, not present in *A. fulgidus* dSiR, are flanking DsrC in Drub, *D. vulgaris* and *D. gigas* Dvir (**Figure 3**), and may play a role in the interaction between DsrAB and DsrC in these proteins.

In Drub, *D. vulgaris* and *D.gigas* Dvir, DsrA shows a 16-residue-insertion (257A–274A), which is partially overlapped by a five-residue longer loop in *A. fulgidus* (119B–125B: *A. fulgidus* numbering). In spite of similar length, the C-terminus of DsrA of both Drub and Dvirs show a different conformation compared to *A. fulgidus* dSiR. In Drub the DsrA C-terminal arm extends along DsrB* (chain E, e.g., distances between Cα atoms: 404A–378E is 4.0 Å, 414A–264E is 4.9 Å, 435A–86D is 5.4 Å) until it reaches DsrA* (chain D) and close to DsrC* (chain F), whereas in *A. fulgidus* the C-terminal arm is more "wrapped" around itself and only in closer contact with DsrB*. These C-terminal tails start diverging after residue 420A (Drub numbering).

Although no 3D structure is yet available for dSiRs belonging to either Desulfofuscidin or P582 classes, we expect similar overall folds for these proteins based on the high sequence identity (ranging from ~50 to 70%) and similarity (ranging from ~65 to 80%) among them. *D. norvegicum* Drub shows highest sequence identity to *D. vulgaris* Dvir (73%), followed by P582 proteins (~65%), and lastly *A. fulgidus* dSiR and Desulfofuscidins (~50%). The DsrA and DsrB cysteine motifs

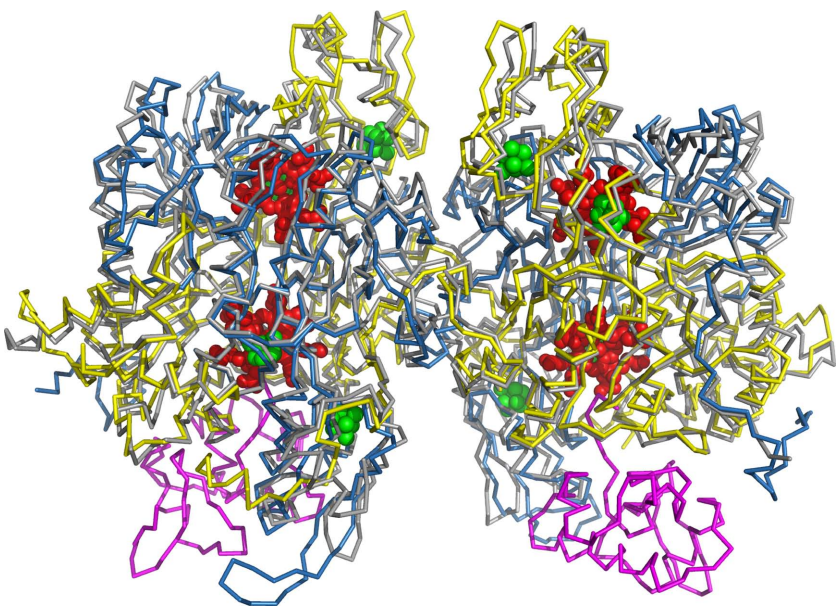

FIGURE 3 | Cα superposition of *D. norvegicum* Drub (DrsA-yellow, DsrB-blue, and DsrC. magenta) and *A. fulgidus* dSiR (gray), structures. For sake of clarity and due to high homology with Drub, the structures of *D. vulgaris* and *D. gigas* Dvirs were not represented. Sirohemes (red) and [4Fe–4S] clusters (green) are drawn in cpk mode (spheres).

required for binding the [4Fe–4S] cluster of the coupled cofactor, as well as the cysteine residues coordinating the ferredoxin domain [4Fe–4S] cluster, are strictly conserved among the analyzed Desulfofuscidin or P582 dSiRs. In addition, most positively charged residues around the catalytic siroheme and surrounding the substrate channel are also conserved in these proteins. Furthermore, the non-conservation of some substrate interacting residues around the non-catalytic DsrA siroheme is also observed in the Desulfofuscidin or P582 dSiRs, which indicates that the presence of a single catalytically active siroheme is a shared characteristic of the different classes of dSirs.

ANALYSIS OF *D. VULGARIS* AND *D. NORVEGICUM* dSiR OLIGOMERIC STATES

As previously reported for *D. vulgaris* Dvir (Lee et al., 1973; Seki et al., 1979; Wolfe et al., 1994; Marritt and Hagen, 1996), as well as recently for *D. gigas* (Hsieh et al., 2010) we observed that purification of Dvir (Oliveira et al., 2008b) and Drub by ion-exchange chromatography originates two or three peaks that cannot be distinguished by several analytical techniques including SDS-PAGE, UV–Visible spectroscopy, and enzyme activity. However, they also originate distinct bands on native gel electrophoresis, which together with the separation by ion-exchange chromatography indicates that they have quite different isoelectric points (Oliveira et al., 2008b).

Native gel of the purified *D. norvegicum* Drub showed three distinct bands, indicating the protein is also present in different states (**Figure 4B**). In *D. vulgaris* Dvir only two bands were observed (**Figure 4A**; Seki et al., 1979; Oliveira et al., 2008b), and crystals could only be obtained from the faster migrating band 1. In order to clarify the difference between the different forms, nanoflow electrospray ionization-mass spectrometry studies of the bands isolated from preparative native gel electrophoresis of *D. vulgaris* and *D. norvegicum* dSiRs were carried out.

The MS spectrum for *D. vulgaris* Dvir band 1 produced well defined peaks corresponding to a MW of 213.8 kDa, indicating the presence of a single species (**Figure 5A**). Analysis of Dvir band 2 from the same gel, provided less definition across the peaks, and a mixture of three species with MW of 213.4, 200.5, and 105.9 kDa is observed (**Figure 5B**). Molecular weight calculations for the different possible stoichiometries between *D. vulgaris* DsrA, DsrB, and DsrC, including cofactors, gives a theoretical MW of 213.3 kDa for the *D. vulgaris* $\alpha_2\beta_2\gamma_2$ form, 200.5 kDa for $\alpha_2\beta_2\gamma$, and 106.6 kDa for $\alpha\beta\gamma$ forms (**Table 2**). From these theoretical masses we can conclude that the fast migrating band 1 of Dvir comprises a single $\alpha_2\beta_2\gamma_2$ species, which is in agreement with the crystal structure obtained. In contrast, the slower migrating Dvir band 2 includes a mixture of three different forms, $\alpha_2\beta_2\gamma_2$ and $\alpha_2\beta_2\gamma$ and $\alpha\beta\gamma$.

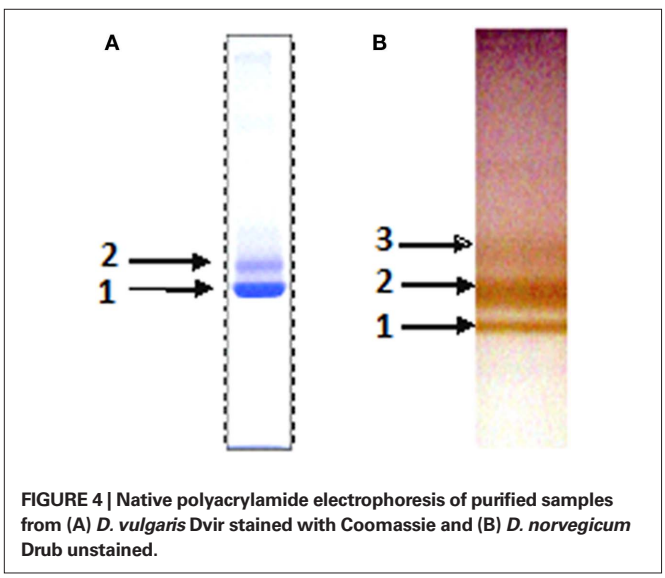

FIGURE 4 | Native polyacrylamide electrophoresis of purified samples from (A) *D. vulgaris* Dvir stained with Coomassie and (B) *D. norvegicum* Drub unstained.

For *D. norvegicum* Drub, bands 1 and 2 produced well defined peaks at 215.1 and 202.0 kDa, respectively, corresponding to single $\alpha_2\beta_2\gamma_2$ (band 1) and $\alpha_2\beta_2\gamma$ (band 2) forms (**Figures 5C,D**). In the slower migrating band 3 (**Figure 5E**), a mixture of peaks at 215.1, 202.3, 189.1, 107.2, and 94.5 kDa is observed, suggesting the presence of an heterogeneous sample corresponding to $\alpha_2\beta_2\gamma_2$, $\alpha_2\beta_2\gamma$, $\alpha_2\beta_2$, $\alpha\beta\gamma$, and $\alpha\beta$ complex compositions. Interestingly, in both Dvir and Drub the dissociation of DsrC is associated with loss of the corresponding siroheme.

Tandem MS experiments were then carried out to try to test dissociation of DsrC from DsrAB in the single species samples, by gradually increasing the trap voltage (**Figure 6**). At 60 V no dissociation is observed, whereas from 80 to 120 V we can detect dissociation of free DsrC, siroheme-bound DsrC as well as siroheme, from the $\alpha_2\beta_2\gamma_2$ and $\alpha_2\beta_2\gamma$ forms of Drub and the $\alpha_2\beta_2\gamma_2$ form of Dvir. The presence of DsrC ions without attached siroheme indicate sub-stoichiometric covalent bonding of this protein to the porphyrin, or disruption of the bond under conditions of collisional activation in the mass spectrometer.

These results are important because they clearly show that the purified dSiRs from *D. vulgaris* and *D. norvegicum*, which seem homogeneous by SDS-PAGE analysis, are in fact a mixture of oligomeric states, even after purification. A similar situation is likely to occur for other purified dSiRs described in the literature, which may explain the disparate results in terms of cofactor content and spectroscopic properties (Rabus et al., 2007), the appearance of several peaks with different pIs in ion-exchange chromatography, and also why this protein resisted attempts to crystallize for so long. The major species present in both Dvir and Drub are the $\alpha_2\beta_2\gamma_2$ and $\alpha_2\beta_2\gamma$ forms. These forms can be separated on ion-exchange chromatography, but the resulting fractions still have some of the other form, probably due to an equilibrium between dissociation and association of the DsrC protein. In addition, the MS results indicate that the crystallization process selects for the $\alpha_2\beta_2\gamma_2$ form with a covalent bond between DsrC and the siroheme, since other forms are present in the Drub protein solution used for crystallization. The presence of the covalent bond is likely to make the whole structure more stable and enable crystallization. Forms of the $\alpha_2\beta_2\gamma_2$ complex without a covalent bond are also likely to be present in the *D. vulgaris* Dvir solution, which did not crystallize. This was confirmed in the *D. gigas* Dvir X-ray structure where non-covalently bonded DsrC is observed, either in a stretched or retracted conformation (Hsieh et al., 2010). In this work the authors could crystallize two of the Dvir forms that are separated by ion-exchange chromatography. In the second form (Dvir-II) one Fe atom is missing, turning the siroheme-associated [4Fe–4S] cluster into a [3Fe–4S] one, and the authors attribute the difference in pI between the two Dvir forms to this fact. We have also observed by EPR that a [3Fe–4S] cluster is present in the slow form of *D. vulgaris* Dvir. However, we consider that this difference alone is

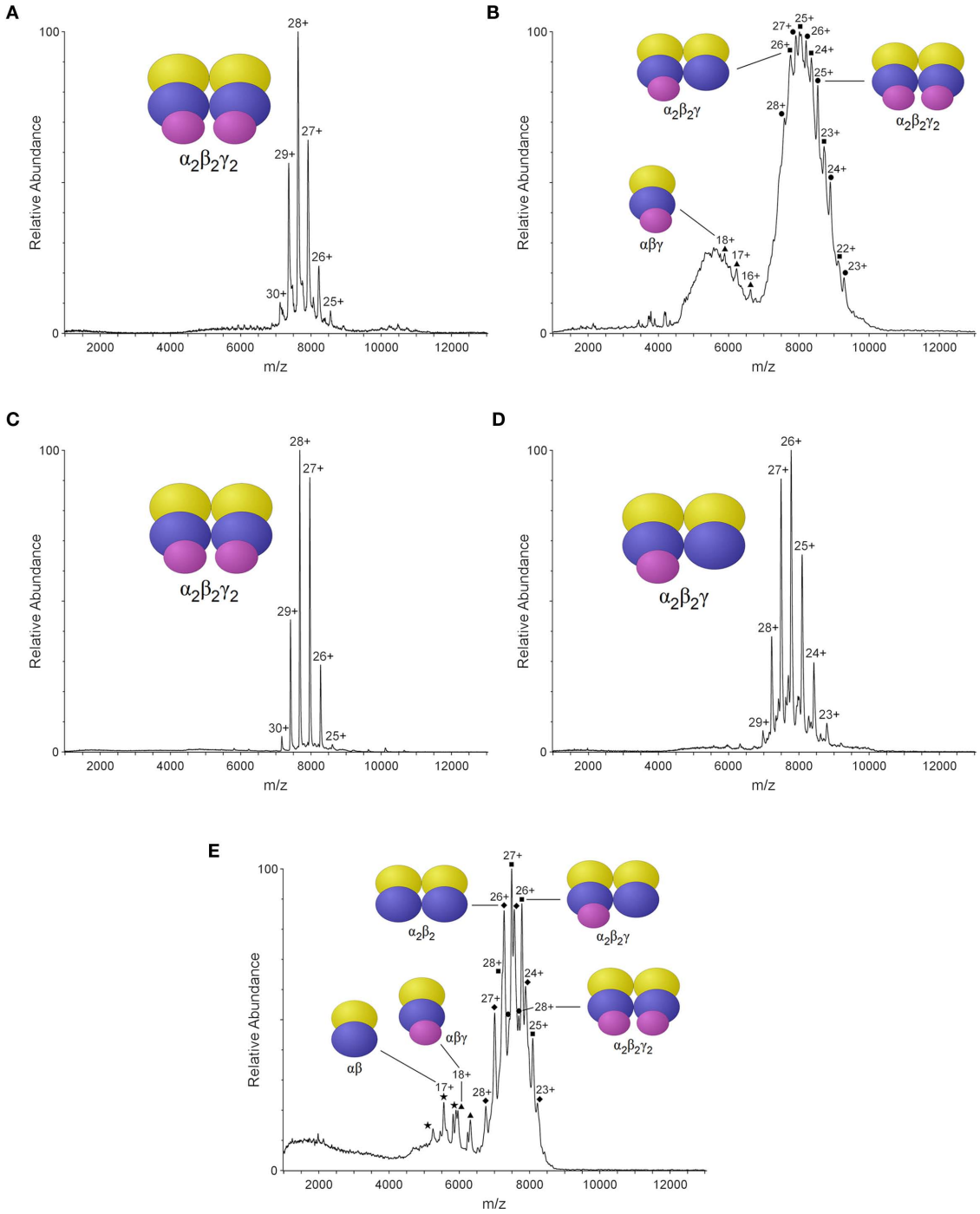

FIGURE 5 | Nano-ESI/MS spectra of the purified dSiRs bands after native gel electrophoresis; *D. vulgaris* Dvir (A) band 1, (B) band 2; *D. norvegicum* (C) band 1, (D) band 2, and (E) band 3. Schematic representation of the different chains as ovals colored as in **Figure 1**.

unlikely to explain the large difference in charge between the two Dvir forms, as the $\alpha_2\beta_2$ complex has a highly negative charge. Rather, it is likely that *D. gigas* Dvir-II separated by ion-chromatography is still a mixture of $\alpha_2\beta_2\gamma$ and $\alpha_2\beta_2\gamma_2$ forms, but the crystallization procedure has selected for the less flexible conformation in the $\alpha_2\beta_2\gamma_2$ form, which is observed in the crystal structure.

SEARCH FOR THE DSIR ELECTRON DONOR

The direct involvement of DsrC in the reduction of sulfite by DsrAB, as revealed by the *D. vulgaris* Dvir structure, led us to propose a mechanism for sulfite reduction in which reduced DsrC is a co-substrate of DsrAB, with oxidized DsrC (with a disulfide bond between the two C-terminal conserved Cys) being

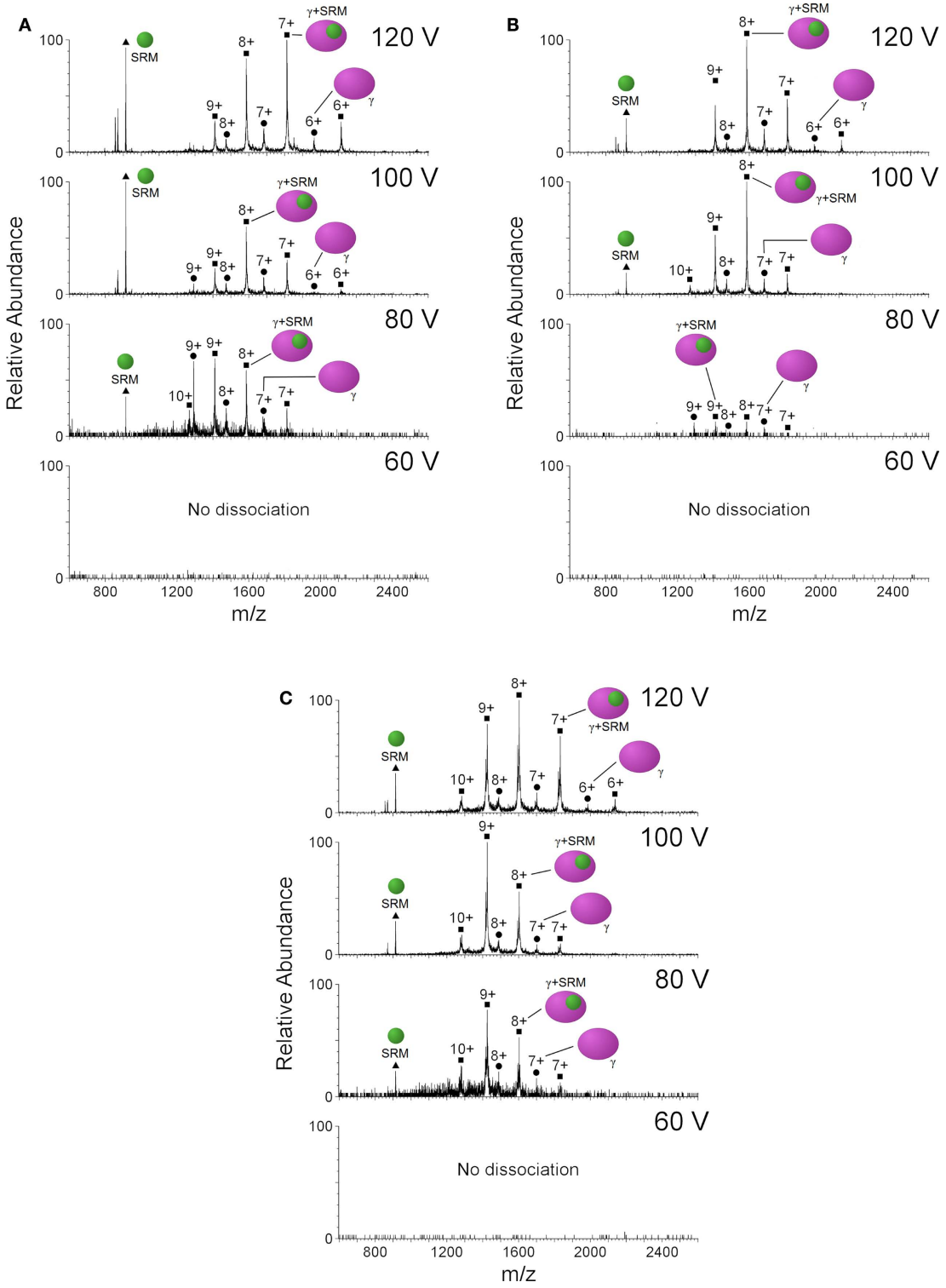

FIGURE 6 | Nano-ESI/MS spectra of (A) band 1 and (B) band 2 from dSiR *D. norvegicum* and for (C) band 1 from *D. vulgaris*, showing the presence of isolated DsrC and SRM and DsrC-SRM complex. Schematic representation of (DsrC) as magenta and siroheme (SRM) as green ovals.

formed as a product (Oliveira et al., 2008a). The oxidized DsrC is proposed to be reduced by the membrane-bound DsrMKJOP complex, with the result that two of the six electrons required for sulfite reduction probably originate from the quinone pool. This still leaves a requirement for another electron donor to deliver the remaining four electrons to dSiR, but this donor has not yet

Table 2 | Predicted and observed molecular weight of the different oligomeric forms of *D. vulgaris* Dvir and *D. norvegicum* Drub.

	Predicted complex stoichiometry	Predicted cofactors	Theoretical MW (kDa)	Obtained MW (kDa)
Dvir band 1	$\alpha_2\beta_2\gamma_2$	2 SRM + 2 SRHC + 8 [4Fe–4S]	213.3	213.8
Dvir band 2	$\alpha_2\beta_2\gamma_2$	2 SRM + 2 SRHC + 8 [4Fe–4S]	213.3	213.4
	$\alpha_2\beta_2\gamma$	1 SRM + 2 SRHC + 8 [4Fe–4S]	200.5	200.5
	$\alpha\beta\gamma$	1 SRM + 1 SRHC + 4 [4Fe–4S]	106.7	105.9
Drub band 1	$\alpha_2\beta_2\gamma_2$	4 SRM + 8 [4Fe–4S]	215.5	215.1
Drub band 2	$\alpha_2\beta_2\gamma$	3 SRM + 8 [4Fe–4S]	202.8	202.0
Drub band 3	$\alpha_2\beta_2\gamma_2$	4 SRM + 8 [4Fe–4S]	215.5	215.1
	$\alpha_2\beta_2\gamma$	3 SRM + 8 [4Fe–4S]	202.8	202.3
	$\alpha_2\beta_2$	2 SRM + 8 [4Fe–4S]	190.0	189.1
	$\alpha\beta\gamma$	2 SRM + 4 [4Fe–4S]	107.8	107.2
	$\alpha\beta$	1 SRM + 4 [4Fe–4S]	95.0	94.5

been identified. It is known that ferredoxin is the electron donor for the aSiRs and nitrite reductases. However, in dSir structures, a ferredoxin domain was incorporated in DsrA and DsrB during dSir evolution (Dahl et al., 1993; Dhillon et al., 2005). This incorporation suggests that the external electron donor may be a ferredoxin-reducing protein.

Using biochemical and biophysical techniques we have tried to examine two potential electron donors to dSiRs: PFOR, and ferredoxin-I. We first generated a model for the *D. vulgaris* Hildenborough PFOR based on the structure of PFOR from *D. africanus* (PDB code 1BOP; Chabriere et al., 2001), since the proteins share 69% sequence identity. The surface electrostatic potential was calculated for both *D. vulgaris* Dvir and PFOR structures, to detect possible interaction sites. On the *D. vulgaris* Dvir surface, a negatively charged region is observed in the ferredoxin domain of chain B, which is a likely region for interaction with an electron donor. In contrast, an overall positive charge along the surface of the ferredoxin domain is observed in PFOR. Using modeling tools in Pymol, the PFOR ferredoxin domain can be placed in the vicinity of the *D. vulgaris* Dvir ferredoxin domain positioning the iron–sulfur clusters of the two domains at ~15 Å from each other. This suggests that electron transfer from the PFOR [4Fe–4S] cluster to the Dvir ferredoxin [4Fe–4S] cluster is possible, so PFOR looks like a plausible candidate electron donor.

We analyzed protein–protein interactions between the *D. vulgaris* Dvir and potential donors using surface plasmon resonance. However, we could detected no direct binding between immobilized Dvir and either PFOR or Fd-I. We cannot exclude that this technique may be hampered by the transient nature of the interaction between PFOR and Dvir. In addition to the direct protein–protein interaction assays, we also tested an activity-based assay for reduction of sulfite by Dvir with pyruvate/PFOR as electron donors. The assay was based on the measurement of sulfide production using the MB method. Again, we could detect no reduction of sulfite from pyruvate. These results do not suggest that PFOR or Fd-I may be physiological electron donors to dSiRs, or alternatively, the system may need other components to allow the enzyme to complete the catalytic cycle. Further work is necessary to elucidate the nature of the electron donor to dSiR.

CONCLUSION

In conclusion, the structure of a Drub determined herein shows that it is similar to the structure of Dvirs. The difference in spectral properties that led to its classification as a different protein is explained by the presence of both sirohydrochlorin and siroheme in Dvir, whereas only siroheme is present in Drub. Since the Drub sirohemes corresponding to the sirohydrochlorins are nonetheless not catalytic, there seems to be little justification for classifying Drub and Dvir as two different classes of dSiRs. The presence of two non-catalytic cofactors in the dSiRs has been confirmed in the four structures reported, where in the *A. fulgidus* dSiR and in the Drub structure reported herein these two cofactors are sirohemes, and in the *D. vulgaris* and *D.gigas* Dvirs they are sirohydrochlorins. The actual function of this cofactor is uncertain. It obviously results from the gene duplication event that gave rise to the homologous DsrA and DsrB subunits, but whereas in the aSiRs this event was followed by loss of this second cofactor (Crane and Getzoff, 1996), in dSiRs this cofactor has been retained. This may either mean that dSiRs are still at an intermediate stage of evolution, which will eventually lead to complete loss of the second cofactor, or that this cofactor has been kept because it is actually performing a valuable function. Since Fe is not required for this function, we tend to favor a structural role for the sirohydrochlorin/siroheme group, which probably serves to stabilize the whole molecule. From sequence and structural analysis we could not identify differences among the dSiRs that could explain why in some cases the Fe is lost, while in others it is retained. Elucidation of the dSiR cofactor insertion and maturation processes may in the future provide further clues to this issue. Schiffer et al. (2008) have also suggested that optimization of the catalytic siroheme site was achieved at the expense of the loss of catalytic activity at the second heme.

Using MS studies we established that purified Dvir and Drub are present in different oligomeric forms with two, one, or no DsrC molecules bound. The relative proportions of these species are likely to be highly dependent on the preparation, finally providing an explanation for the conflicting results in terms of cofactor content and spectroscopy results for these proteins. In addition, we obtained evidence for the fact that not all DsrC molecules in the DsrABC complexes have a covalent bond to the siroheme (as was recently confirmed by the *D. gigas* Dvir structures), which further

supports the involvement of the DsrC penultimate Cys in the sulfite reduction mechanism. Our preliminary attempts to discover the physiological electron donor to dSir have proved unsuccessful, and future studies are necessary to elucidate this important question.

ACKNOWLEDGMENTS

This work was supported by research grant PTDC/QUI-BIQ/100591/2008 to Inês A. C. Pereira and PTDC/BIA-PRO/103718/2008 to Margarida Archer funded by Fundação para a Ciência e Tecnologia (FCT, MCTES, Portugal); and by a Science Foundation Ireland Investigator grant (07/IN.1/B975) to Amir R. Khan, Edward Franklin and Tânia F. Oliveira. FCT is acknowledged for the fellowship to Tânia F. Oliveira (SFRH/BD/29519/2006) and ESRF for financial and technical support for X-ray diffraction data collection. We thank Dr. Pedro Matias for help in refinement and fruitful discussions. We acknowledge Dr. Chun-Jung Chen (Taiwan) for providing us the coordinates of *D. gigas* Dvir with the retracted DsrC C-terminal arm.

REFERENCES

Akagi, J. M., Chan, M., and Adams, V. (1974). Observations on the bisulfite reductase (P582) isolated from *Desulfotomaculum nigrificans*. *J. Bacteriol.* 120, 240–244.

Arendsen, A. F., Verhagen, M. F., Wolbert, R. B., Pierik, A. J., Stams, A. J., Jetten, M. S., and Hagen, W. R. (1993). The dissimilatory sulfite reductase from *Desulfosarcina variabilis* is a desulforubidin containing uncoupled metalated sirohemes and S = 9/2 iron-sulfur clusters. *Biochemistry* 32, 10323–10330.

Canfield, D. E., and Raiswell, R. (1999). The evolution of the sulfur cycle. *Am. J. Sci.* 299, 627–723.

Canfield, D. E., Rosing, M. T., and Bjerrum, C. (2006). Early anaerobic metabolisms. *Philos. Trans. R. Soc. Lond. B Biol. Sci.* 361, 1819–1834; discussion 1835–1836.

Chabriere, E., Vernede, X., Guigliarelli, B., Charon, M. H., Hatchikian, E. C., and Fontecilla-Camps, J. C. (2001). Crystal structure of the free radical intermediate of pyruvate:ferredoxin oxidoreductase, *Science* 294, 2559–2563.

Collaborative Computational Project, Number 4. (1994). The CCP4 suite: programs for protein crystallography. *Acta Crystallogr. D Biol. Crystallogr.* 50, 760–763.

Cort, J. R., Mariappan, S. V., Kim, C. Y., Park, M. S., Peat, T. S., Waldo, G. S., Terwilliger, T. C., and Kennedy, M. A. (2001). Solution structure of *Pyrobaculum aerophilum* DsrC, an archaeal homologue of the gamma subunit of dissimilatory sulfite reductase. *Eur. J. Biochem.* 268, 5842–5850.

Cort, J. R., Selan, U., Schulte, A., Grimm, F., Kennedy, M. A., and Dahl, C. (2008). *Allochromatium vinosum* DsrC: solution-state NMR structure, redox properties, and interaction with DsrEFH, a protein essential for purple sulfur bacterial sulfur oxidation. *J. Mol. Biol.* 382, 692–707.

Cowtan, K. (2006). The Buccaneer software for automated model building. 1. Tracing protein chains. *Acta Crystallogr. D Biol. Crystallogr.* 62, 1002–1011.

Crane, B. R., and Getzoff, E. D. (1996). The relationship between structure and function for the sulfite reductases. *Curr. Opin. Struct. Biol.* 6, 744–756.

Crane, B. R., Siegel, L. M., and Getzoff, E. D. (1995). Sulfite reductase structure at 1.6 A: evolution and catalysis for reduction of inorganic anions. *Science* 270, 59–67.

Dahl, C., Engels, S., Pott-Sperling, A. S., Schulte, A., Sander, J., Lubbe, Y., Deuster, O., and Brune, D. C. (2005). Novel genes of the dsr gene cluster and evidence for close interaction of Dsr proteins during sulfur oxidation in the phototrophic sulfur bacterium *Allochromatium vinosum*. *J. Bacteriol.* 187, 1392–1404.

Dahl, C., Kredich, N. M., Deutzmann, R., and Truper, H. G. (1993). Dissimilatory sulphite reductase from *Archaeoglobus fulgidus*: physico-chemical properties of the enzyme and cloning, sequencing and analysis of the reductase genes. *J. Gen. Microbiol.* 139, 1817–1828.

DeLano, W. L. (2002). *The PyMOL Molecular Graphics System*. San Carlos, CA: DeLano Scientific.

DerVartanian, D. V. (1994). Desulforubidin: dissimilatory, high-spin sulfite reductase of *Desulfomicrobium* species. *Meth. Enzymol.* 243, 270–276.

Dhillon, A., Goswami, S., Riley, M., Teske, A., and Sogin, M. (2005). Domain evolution and functional diversification of sulfite reductases. *Astrobiology* 5, 18–29.

Emsley, P., and Cowtan, K. (2004). Coot: model-building tools for molecular graphics. *Acta Crystallogr. D Biol. Crystallogr.* 60, 2126–2132.

Fogo, J. K., and Milton, P. (1949). Spectrophotometric determination of hydrogen sulfide. *Anal. Chem.* 21, 732–734.

Hatchikian, E. C. (1994). Desulfofuscidin: dissimilatory, high-spin sulfite reductase of thermophilic, sulfate-reducing bacteria. *Meth. Enzymol.* 243, 276–295.

Hatchikian, E. C., and Zeikus, J. G. (1983). Characterization of a new type of dissimilatory sulfite reductase present in *Thermodesulfobacterium commune*. *J. Bacteriol.* 153, 1211–1220.

Hsieh, Y. C., Liu, M. Y., Wang, V. C., Chiang, Y. L., Liu, E. H., Wu, W. G., Chan, S. I., and Chen, C. J. (2010). Structural insights into the enzyme catalysis from comparison of three forms of dissimilatory sulphite reductase from *Desulfovibrio gigas*. *Mol. Microbiol.* 78, 1101–1116.

Ikeuchi, Y., Shigi, N., Kato, J., Nishimura, A., and Suzuki, T. (2006). Mechanistic insights into multiple sulfur mediators sulfur relay by involved in thiouridine biosynthesis at tRNA wobble positions. *Mol. Cell* 21, 97–108.

Klein, M., Friedrich, M., Roger, A. J., Hugenholtz, P., Fishbain, S., Abicht, H., Blackall, L. L., Stahl, D. A., and Wagner, M. (2001). Multiple lateral transfers of dissimilatory sulfite reductase genes between major lineages of sulfate-reducing prokaryotes. *J. Bacteriol.* 183, 6028–6035.

Krissinel, E., and Henrick, K. (2004). Secondary-structure matching (SSM), a new tool for fast protein structure alignment in three dimensions. *Acta Crystallogr. D Biol. Crystallogr.* 60, 2256–2268.

Laskowski, R. A., MacArthur, M. W., Moss, D. S., and Thornton, J. M. (1993). PROCHECK: a program to check the stereochemical quality of protein structures. *J. Appl. Crystallogr.* 26, 283–291.

Lee, J. P., and Peck, H. D. (1971). Purification of the enzyme reducing bisulfite to trithionate from *Desulfovibrio gigas* and its identification as desulfoviridin. *Biochem. Biophys. Res. Commun.* 45, 583–589.

Lee, J. P., Yi, C.-S., LeGall, J., and Peck, H. D. (1973). Isolation of a new pigment, desulforubidin, from *Desulfovibrio desulfuricans* (Norway strain) and its role in sulfite reduction. *J. Bacteriol.* 115, 453–455.

Leslie, A. G. W. (1992). *Joint CCP4+ESF-EAMBC Newsletter on Protein Crystallography 26.*

Loy, A., Duller, S., and Wagner, M. (2007). "Evolution and ecology of microbes dissimilating sulfur compounds: insights from siroheme sulfite reductases," in *Microbial Sulfur Metabolism*, eds C. Dahl and C. Friedrich (Berlin: Springer), 46–59.

Mander, G. J., Weiss, M. S., Hedderich, R., Kahnt, J., Ermler, U., and Warkentin, E. (2005). X-ray structure of the gamma-subunit of a dissimilatory sulfite reductase: fixed and flexible C-terminal arms. *FEBS Lett.* 579, 4600–4604.

Marritt, S. J., and Hagen, W. F. (1996). Dissimilatory sulfite reductase revisited. The desulfoviridin molecule does contain 20 iron ions, extensively demetallated siroheme, and an S = 9/2 iron-sulfur cluster. *Eur. J. Biochem.* 238, 724–727.

Matthews, B. W. (1968). Solvent content of protein crystals. *J. Mol. Biol.* 33, 491–497.

McCoy, A. J., Grosse-Kunstleve, R. W., Adams, P. D., Winn, M. D., Storoni, L. C., and Read, R. J. (2007). Phaser crystallographic software. *J. Appl. Crystallogr.* 40, 658–674.

Molitor, M., Dahl, C., Molitor, I., Schafer, U., Speich, N., Huber, R., Deutzmann, R., and Truper, H. G. (1998). A dissimilatory siroheme-sulfite-reductase-type protein from the hyperthermophilic archaeon *Pyrobaculum islandicum*. *Microbiology* 144(Pt 2), 529–541.

Moura, I., LeGall, J., Lino, A. R., Peck, H. D., Fauque, G., Xavier, A. V., DerVartanian, D. V., Moura, J. J. G., and Huynh, B. H. (1988). Characterization of two dissimilatory sulfite reductases (desulforubidin and desulfoviridin) from the sulfate-reducing bacteria. Mössbauer and EPR Studies. *J. Am. Chem. Soc.* 110, 1075–1082.

Murshudov, G. N., Vagin, A. A., and Dodson, E. J. (1997). Refinement of macromolecular structures by the maximum-likelihood method. *Acta Crystallogr. D Biol. Crystallogr.* 53, 240–255.

Numata, T., Fukai, S., Ikeuchi, Y., Suzuki, T., and Nureki, O. (2006). Structural basis for sulfur relay to RNA mediated by heterohexameric TusBCD complex. *Structure* 14, 357–366.

Oliveira, T. F., Vonrhein, C., Matias, P. M., Venceslau, S. S., Pereira, I. A., and Archer, M. (2008a). The crystal structure of *Desulfovibrio vulgaris* dissimilatory sulfite reductase bound to DsrC provides novel insights into the mechanism of sulfate respiration. *J. Biol. Chem.* 283, 34141–34149.

Oliveira, T. F., Vonrhein, C., Matias, P. M., Venceslau, S. S., Pereira, I. A., and Archer, M. (2008b). Purification, crystallization and preliminary crystallographic analysis of a dissimilatory DsrAB sulfite reductase in complex with DsrC. *J. Struct. Biol.* 164, 236–239.

Parey, K., Warkentin, E., Kroneck, P. M., and Ermler, U. (2010). Reaction cycle of the dissimilatory sulfite reductase from *Archaeoglobus fulgidus*. *Biochemistry* 49, 8912–8921.

Peck, H. D. Jr., and LeGall, J. (1982). Biochemistry of dissimilatory sulphate reduction. *Philos. Trans. R. Soc. Lond. B Biol. Sci.* 298, 443–466.

Pereira, P. M., Teixeira, M., Xavier, A. V., Louro, R. O., and Pereira, I. A. C. (2006). The Tmc complex from *Desulfovibrio vulgaris* Hildenborough is involved in transmembrane electron transfer from periplasmic hydrogen oxidation. *Biochemistry* 45, 10359–10367.

Pierik, A. J., Duyvis, M. G., van Helvoort, J. M., Wolbert, R. B., and Hagen, W. R. (1992). The third subunit of desulfoviridin-type dissimilatory sulfite reductases. *Eur. J. Biochem.* 205, 111–115.

Pierik, A. J., and Hagen, W. R. (1991). S = 9/2 EPR signals are evidence against coupling between the siroheme and the Fe/S cluster prosthetic groups in *Desulfovibrio vulgaris* (Hildenborough) dissimilatory sulfite reductase. *Eur. J. Biochem.* 195, 505–516.

Pires, R. H., Venceslau, S. S., Morais, F., Teixeira, M., Xavier, A. V., and Pereira, I. A. C. (2006). Characterization of the *Desulfovibrio desulfuricans* ATCC 27774 DsrMKJOP complex – a membrane-bound redox complex involved in sulfate respiration. *Biochemistry* 45, 249–262.

Rabus, R., Hansen, T., and Widdel, F. (2007). "Dissimilatory sulfate- and sulfur-reducing prokaryotes," in *The Prokaryotes*, ed. M. E. A. Dworkin (New York: Springer-Verlag), 659–768.

Schiffer, A., Parey, K., Warkentin, E., Diederichs, K., Huber, H., Stetter, K. O., Kroneck, P. M., and Ermler, U. (2008). Structure of the dissimilatory sulfite reductase from the hyperthermophilic archaeon *Archaeoglobus fulgidus*. *J. Mol. Biol.* 379, 1063–1074.

Schnell, R., Sandalova, T., Hellman, U., Lindqvist, Y., and Schneider, G. (2005). Siroheme- and [Fe4-S4]-dependent NirA from *Mycobacterium tuberculosis* is a sulfite reductase with a covalent Cys-Tyr bond in the active site. *J. Biol. Chem.* 280, 27319–27328.

Seki, Y., Kobayashi, K., and Ishimoto, M. (1979). Biochemical studies on sulfate-reducing bacteria. XV. Separation and comparison of two forms of desulfoviridin. *J. Biochem.* 85, 705–711.

Steuber, J., Arendsen, A. F., Hagen, W. R., and Kroneck, P. M. (1995). Molecular properties of the dissimilatory sulfite reductase from *Desulfovibrio desulfuricans* (Essex) and comparison with the enzyme from *Desulfovibrio vulgaris* (Hildenborough). *Eur. J. Biochem.* 233, 873–879.

Steuber, J., Cypionka, H., and Kroneck, P. M. H. (1994). Mechanism of dissimilatory sulfite reduction by *Desulfovibrio desulfuricans* – purification of a membrane-bound sulfite reductase and coupling with cytochrome C(3) and hydrogenase. *Arch. Microbiol.* 162, 255–260.

Swamy, U., Wang, M., Tripathy, J. N., Kim, S. K., Hirasawa, M., Knaff, D. B., and Allen, J. P. (2005). Structure of spinach nitrite reductase: implications for multi-electron reactions by the iron-sulfur:siroheme cofactor. *Biochemistry* 44, 16054–16063.

Wagner, M., Roger, A. J., Flax, J. L., Brusseau, G. A., and Stahl, D. A. (1998). Phylogeny of dissimilatory sulfite reductases supports an early origin of sulfate respiration. *J. Bacteriol.* 180, 2975–2982.

Weiss, M. S., Mander, G., Hedderich, R., Diederichs, K., Ermler, U., and Warkentin, E. (2004). Determination of a novel structure by a combination of long-wavelength sulfur phasing and radiation-damage-induced phasing. *Acta Crystallogr. D Biol. Crystallogr.* 60, 686–695.

Wolfe, B. M., Lui, S. M., and Cowan, J. A. (1994). Desulfoviridin, a multimeric-dissimilatory sulfite reductase from *Desulfovibrio vulgaris* (Hildenborough). Purification, characterization, kinetics and EPR studies. *Eur. J. Biochem.* 223, 79–89.

Zverlov, V., Klein, M., Lucker, S., Friedrich, M. W., Kellermann, J., Stahl, D. A., Loy, A., and Wagner, M. (2005). Lateral gene transfer of dissimilatory (bi) sulfite reductase revisited. *J. Bacteriol.* 187, 2203–2208.

Conflict of Interest Statement: The authors declare that the research was conducted in the absence of any commercial or financial relationships that could be construed as a potential conflict of interest.

Received: 09 February 2011; paper pending published: 25 February 2011; accepted: 28 March 2011; published online: 13 April 2011.

*Citation: Oliveira TF, Franklin E, Afonso JP, Khan AR, Oldham NJ, Pereira IAC and Archer M (2011) Structural insights into dissimilatory sulfite reductases: structure of desulforubidin from Desulfomicrobium norvegicum. Front. Microbio. **2**:71. doi: 10.3389/fmicb.2011.00071*

This article was submitted to Frontiers in Microbial Physiology and Metabolism, a specialty of Frontiers in Microbiology.